

Article

Preparation of Bamboo-Based Hierarchical Porous Carbon Modulated by FeCl₃ towards Efficient Copper Adsorption

Yixin Zhang ^{1,2,*}, Guofeng Qiu ^{3,†}, Rumeng Wang ³, Yang Guo ³ , Fanhui Guo ³  and Jianjun Wu ^{3,*}

¹ National Engineering Research Center of Coal Preparation and Purification, China University of Mining and Technology, No.1 Daxue Road, Xuzhou 221116, China

² Shandong Xuanyuan Scientific Engineering and Industrial Technology Research Institute Co., Ltd., Longgu, Juye, Heze 274918, China

³ School of Chemical Engineering and Technology, China University of Mining and Technology, No.1 Daxue Road, Xuzhou 221116, China; ts20040045a31@cumt.edu.cn (G.Q.); rumengwang@cumt.edu.cn (R.W.); cumt-guoyang@cumt.edu.cn (Y.G.); cumtgh@163.com (F.G.)

* Correspondence: yixinzhang@cumt.edu.cn (Y.Z.); jjuw@163.com (J.W.);
Tel.: +86-152-62-190-991 (Y.Z.); +86-139-51-350-506 (J.W.)

† Yixin Zhang and Guofeng Qiu contributed equally to this work.

Abstract: Using bamboo powder biochar as raw material, high-quality meso/microporous controlled hierarchical porous carbon was prepared—through the catalysis of Fe³⁺ ions loading, in addition to a chemical activation method—and then used to adsorb copper ions in an aqueous solution. The preparation process mainly included two steps: load-alkali leaching and chemical activation. The porosity characteristics (specific surface area and mesopore ratio) were controlled by changing the K₂CO₃ impregnation ratio, activation temperature, and Fe³⁺ ions loading during the activation process. Additionally, three FBPC samples with different pore structures and characteristics were studied for copper adsorption. The results indicate that the adsorption performance of the bamboo powder biochar FBPC material was greatly affected by the meso/micropore ratio. FBPC 2.5-900-2%, impregnated at a K₂CO₃: biochar ratio of 2.5 and a Fe³⁺: biochar mass ratio of 2%, and activated at 900 °C for 2 h in N₂ atmosphere, has a very high specific surface area of 1996 m² g⁻¹ with a 58.1% mesoporous ratio. Moreover, it exhibits an excellent adsorption capacity of 256 mg g⁻¹ and rapid adsorption kinetics for copper ions. The experimental results show that it is feasible to control the hierarchical pore structure of bamboo biochar-derived carbons as a high-performance adsorbent to remove copper ions from water.

Keywords: bamboo powder; biochar; hierarchical porous carbon; Fe³⁺ ions; adsorption; copper ions



Citation: Zhang, Y.; Qiu, G.; Wang, R.; Guo, Y.; Guo, F.; Wu, J. Preparation of Bamboo-Based Hierarchical Porous Carbon Modulated by FeCl₃ towards Efficient Copper Adsorption. *Molecules* **2021**, *26*, 6014. <https://doi.org/10.3390/molecules26196014>

Academic Editors: Carlo Santoro, Binglin Guo, Quanzhi Tian and Chuncai Zhou

Received: 20 August 2021

Accepted: 30 September 2021

Published: 3 October 2021

Publisher's Note: MDPI stays neutral with regard to jurisdictional claims in published maps and institutional affiliations.



Copyright: © 2021 by the authors. Licensee MDPI, Basel, Switzerland. This article is an open access article distributed under the terms and conditions of the Creative Commons Attribution (CC BY) license (<https://creativecommons.org/licenses/by/4.0/>).

1. Introduction

Heavy metal pollution of water has been a challenge in many countries around the world for decades and has attracted the attention of researchers due to its serious impact on human health. Because the removal of heavy metals usually requires expensive materials and complex methods, the use of low-cost and environmentally friendly waste forest products is a simple and effective approach. At present, among the heavy metals with toxic effects on humans and the environment, the sources of copper ions can be divided into natural and man-made, such as volcanic activity, mining, and smelting, brass manufacturing, electroplating, oil refining, etc., and exist in the aquatic environment, which grants easy entry into the food chain [1]. According to the World Health Organization, the maximum concentration of copper in drinking water in many countries is 3.0 mg L⁻¹ [2]. In the human body, copper is retained by homeostasis [3]. Excessive concentrations of copper ions in the human body can lead to kidney/liver damage as well as Alzheimer's disease [4]. Many conventional methods, including electrochemical methods, chemical precipitation, chemical coagulation, membrane filtration, ion exchange, and bioremediation, have been

used to remove copper from natural water sources and wastewater [5–8]. However, most of these treatment techniques are environmentally damaging and suffer from lower efficiency, operational limitations, and high cost, all of which restrict their application. Compared with other technologies, adsorption is considered to be the most effective physical and chemical technology to remove heavy metals because of its simple operation, cost-effectiveness, and the regeneration properties of the adsorbent [9]. Many studies on the adsorption of copper by activated carbon and waste biomass adsorbents have been carried out [10–12]. It is worth noting that in the adsorption process, the adsorbent is considered to be the most important factor affecting the removal efficiency of pollutants. Therefore, it is very important to find a cost-effective and environmentally friendly adsorbent to remove copper.

In recent years, the application of biomass resources in the preparation of porous carbon materials has attracted much attention because of its renewability. As waste from the paper industry, bamboo powder has the advantage of being economical and widely available. In addition, hierarchical porous carbon has interesting advantages due to its special structure [10,13], so there have been a lot of studies related to it. Interconnections among macropores, mesopores, and micropores within hierarchical porous carbon structures facilitate rapid ion transport [14]. Macropores and mesopores promote rapid ion transfer through channels to micropores [15], resulting in rapid mass transfer kinetics and low mass transfer resistance [12].

Bamboo is composed of cellulose, hemicellulose, and lignin. The carbonization of lignocellulosic components mainly results in the formation of micropores [16]. To obtain the typical char structure mentioned above, Fe-based compounds are used for the following reasons. First, Fe-based compounds (such as Fe_2O_3 and FeCl_3) can be used as templates to synthesize mesoporous materials [17,18]. Mixtures containing biomass carbon and metallic compounds are heated to high temperatures. After pyrolysis, the metal compounds in biomass carbon can be easily removed with diluted hydrochloric acid and a clear mesoporous structure can be obtained. Secondly, iron-based compounds can also improve the microstructure. Xu et al. [19] and Oztas et al. [20] showed that iron-based compounds could catalyze the decomposition of all hydrocarbons in biomass carbon, with the exception of methane. This reaction promotes the formation and release of volatiles and hinders the condensation of free radicals during pyrolysis. Finally, iron is a common natural ingredient, and it has a lower cost than other metals such as vanadium, nickel, and zirconium. Therefore, the preparation of a typical biomass charcoal material in the pyrolysis process can be achieved by changing the amount of iron-based compounds. These factors play an important role in determining the development of pores during activation, but they are rarely discussed systematically.

In this study, using bamboo powder biochar as a raw material and FeCl_3 and K_2CO_3 as additives, the effects of different contents of FeCl_3 and K_2CO_3 on the pore structure (the specific surface area and the $V_{\text{meso}}/V_{\text{total}}$ ratio) and the physical and chemical properties of FBPC samples were studied. In addition, the effects of the adsorption isotherm, kinetics, and initial pH on the adsorption of copper ions on different FBPC materials were studied through batch experiments to determine the adsorption behavior of copper ions on different FBPC materials.

2. Results and Discussion

BC was prepared by carbonizing bamboo powder in a process in which the pyrolysis of the organic components of the feedstock included the release of oxygen and hydrogen as carbon monoxide, carbon dioxide, H_2 and H_2O , and condensable volatiles to obtain the carbon material [21]. FBPC was then manufactured through supported Fe^{3+} ion catalysis and a chemical activation process to improve the porous structure by eliminating remaining inorganic and amorphous carbon [22].

2.1. Physical Characteristics

The physical properties of the material were studied to estimate the porosity development within the BC to form a hierarchical porous structure in the FBPC sample. The specific surface area, total pore volume, and pore width of BC, BPC, and FBPC samples were determined by nitrogen sorption and desorption. The nitrogen adsorption–desorption isotherms and pore size distributions are shown in Figure 1a–c. As shown in the figure, the FBPC 2.5-900-1%, FBPC 2.5-900-2%, FBPC 2.5-900-4%, and BPC 2.5-900 (FBPC 2.5-900-0%) samples all belonged to type I isotherms and type H4 hysteresis loops, suggesting that micropores and mesopores coexisted [15,22]. The most interesting aspect was the apparent hysteresis of the rings in the FBPC 2.5-900-1%, FBPC 2.5-900-2%, and FBPC 2.5-900-4% samples, but for BPC 2.5-900, no such rings were observed. This difference indicated that FBPC 2.5-900-1%, FBPC 2.5-900-2%, and FBPC 2.5-900-4% samples had a higher number of mesopores. In addition, the density function theoretical model was used to calculate the pore size distribution of FBPC samples. All FBPC samples loaded with Fe^{3+} ions mainly consisted of micropores in the range of 0.6 to 2.0 nm and mesoporous pores in the range of 2.0 to 7 nm. However, the mesoporous range of BPC 2.5-900 (FBPC 2.5-900-0%) was mainly 2 to 5 nm.

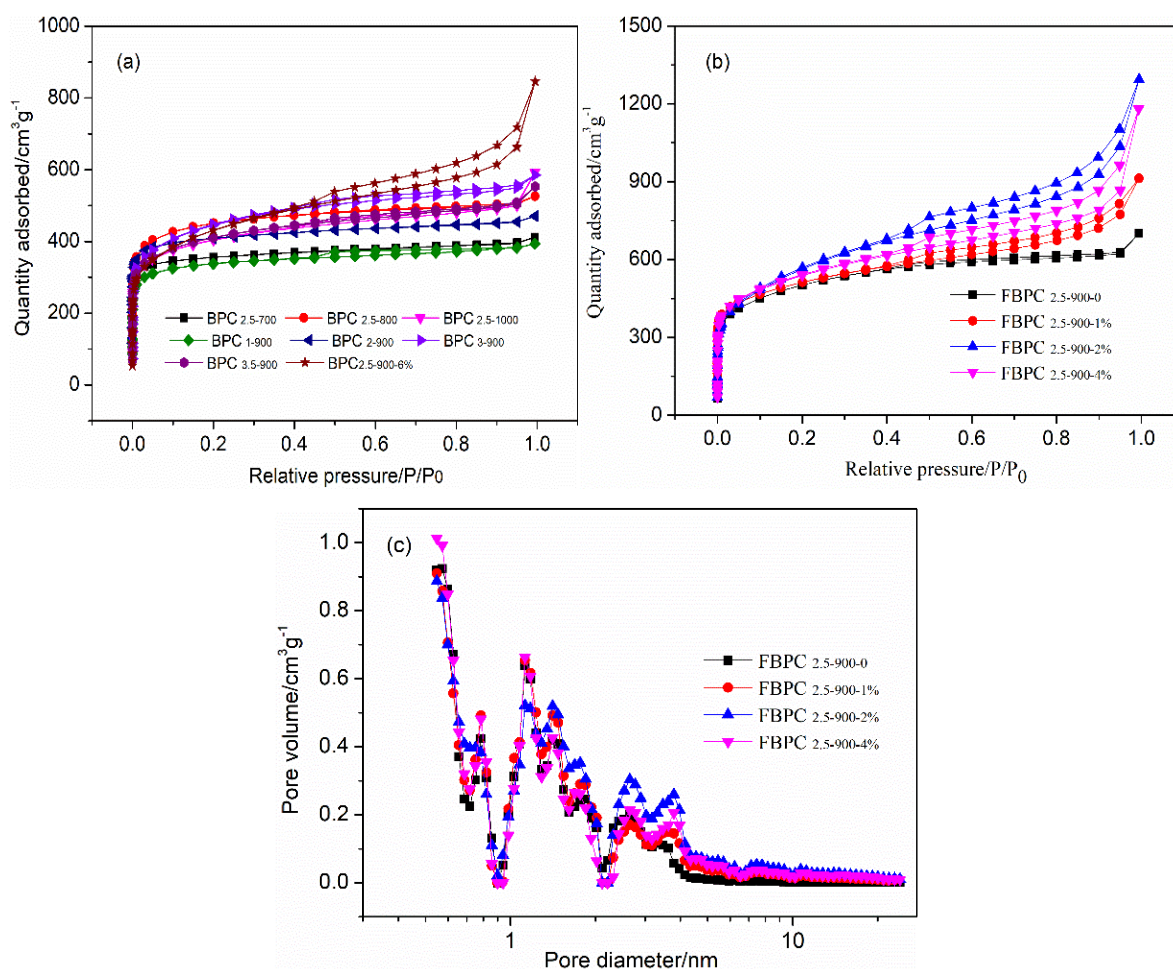


Figure 1. (a) Nitrogen adsorption/desorption isotherms of the BPC and FBPC samples; (b) nitrogen adsorption/desorption isotherms; and (c) DFT pore size distribution of the FBPC samples.

The results in Table 1 show that the specific surface area of the BC sample was only $468 \text{ m}^2 \text{ g}^{-1}$ after the carbonization step of the organic compound was removed. By using chemical activation and catalytic processes, the specific surface area of the BPC samples was significantly increased, i.e., it was in the range of 1301 to $1996 \text{ m}^2 \text{ g}^{-1}$. At the same time, the ratio of mesopore to total pore volume ($V_{\text{meso}}/V_{\text{total}}$) ranged from 0.11 to 0.581. Therefore,

FBPC samples with high specific surface area and adjustable mesoporous/microporous ratio can be prepared by controlling three operating parameters during the activation process: the temperature, the K_2CO_3 to BC ratio, and amount of $FeCl_3$ added.

Table 1. Summary of the pore characterization data of the BC, BPC, and FBPC samples.

Adsorbent	S_{BET}^a ($m^2 g^{-1}$)	V_{total}^b ($cm^3 g^{-1}$)	V_{micro}^c ($cm^3 g^{-1}$)	V_{meso}^d ($cm^3 g^{-1}$)	$V_{micro}/V_{total} \%$	$V_{meso}/V_{total} \%$	$D_{ave}(nm)$
BC	468	0.303	0.154	0.149	50.8	49.2	2.921
BPC 2.5-700	1405	0.582	0.518	0.064	89.0	11.0	1.913
BPC 2.5-800	1688	0.729	0.626	0.103	85.9	14.1	2.130
BPC 2.5-900	1793	0.894	0.615	0.279	68.8	31.2	2.414
BPC 2.5-1000	1528	0.724	0.532	0.192	73.4	26.6	2.435
BPC 1-900	1301	0.556	0.478	0.078	86.0	14.0	1.872
BPC 2-900	1607	0.760	0.588	0.172	77.3	22.7	2.232
BPC 3-900	1612	0.798	0.569	0.229	71.3	28.7	2.246
BPC 3.5-900	1508	0.729	0.537	0.192	73.7	26.3	2.268
FBPC 2.5-900-1%	1823	1.265	0.608	0.657	48.1	51.9	3.685
FBPC 2.5-900-2%	1996	1.571	0.659	0.912	41.9	58.1	3.890
FBPC 2.5-900-4%	1894	1.380	0.618	0.762	44.8	55.2	3.792
FBPC 2.5-900-6%	1537	0.935	0.492	0.443	52.6	47.4	3.603

^a BET—specific surface area. ^b total volume of pores. ^c volume of micropores. ^d volume of mesopores.

It was obvious that the activation temperature was one of the key factors for the specific surface area and pore volume of strong BPC samples. The specific surface area of BPC samples increased from $1405 m^2 g^{-1}$ of BPC 2.5-700 to $1793 m^2 g^{-1}$ of BPC 2.5-900, which corresponded to activation temperatures of $700 ^\circ C$ and $900 ^\circ C$, respectively. Notably, the V_{meso}/V_{total} of the BPC 2.5-700 and BPC 2.5-900 samples was 0.11 and 0.312, respectively, indicating a significant enhancement of mesopore. The increase in pore structure in the BPC sample was most likely due to the widening of the micropores towards the mesopores [23]. However, when the temperature continued to rise from $900 ^\circ C$ to $1000 ^\circ C$, the specific area and pore volume decreased (the total specific surface area decreased from $1996 m^2 g^{-1}$ to $1528 m^2 g^{-1}$, and V_{total} decreased from 0.894 to 0.724), but the pore size increased. This was the case because higher activation temperatures lead to more carbon atoms being involved in the reaction, and larger numbers of etched pores lead to more metal potassium turning into vapor (the boiling point of potassium is $762 ^\circ C$) and entering the middle of the carbon layer for further etching. This reaction can broaden the radius of the hole, while it will also break the generated pore structure, resulting in the collapse of some pores, and thus, the specific surface area and pore volume of the obtained material will decrease. In addition, the impregnation ratio of K_2CO_3 : BC affected the generation of new pores, widened existing pores, and controlled the ratio of mesopores to micropores. At $900 ^\circ C$, the specific surface area increased significantly from $1301 m^2 g^{-1}$ in the BPC 1-900 sample to $1793 m^2 g^{-1}$ in the BPC 2.5-900 sample, and the V_{meso}/V_{total} increased from 0.14 to 0.312. However, when the K_2CO_3 : BPC ratio further increased to 3.5 in the BPC 3.5-900 sample, the specific surface area gradually decreased, but the V_{meso}/V_{total} decreased to 0.263. This reduction may have been due to excess K_2CO_3 reacting with carbon atoms to convert carbon dioxide in a gaseous form, with some mesopores collapsing during the activation time period [11,24].

From Figure 1b,c, and Table 1, it can be seen that an increase in Fe^{3+} ions loading from 0% to 2% led to an increase in the specific surface area, mesopore volume, and V_{meso}/V_{total} . However, for the FBPC 2.5-900-2% and FBPC 2.5-900-6% samples, the loading of Fe^{3+} ions increased from 2% to 6%, the total specific surface area decreased from $1996 m^2 g^{-1}$ to $1537 m^2 g^{-1}$, and the V_{meso}/V_{total} value decreased from 0.581 to 0.474. From these results, it can be concluded that with the increase in the loading capacity, the adsorption curve was gradually warped upward. From the pore size distribution and pore structure parameters, it can be seen that the micropore volume of different pore sizes (0–2 nm) increased signifi-

cantly with the increase in the micropore diameter of iron-carrying precursors, and the total pore volume also continued to increase. The pore reaming of the micropores also generated a part of the mesopores, resulting in a rapid increase in the specific surface area. The results show that the presence of iron compounds in the activation process inhibited the growth of aromatic lamellae and their longitudinal polycondensation behavior, promoted the further cracking of large aromatic rings to small aromatic rings and the generation of active sites, weakened the diffusion resistance of activated gases in the particles, and fully etched the microcrystalline structure to generate a large number of new micropores and mesopores [25]. For FBPC_{2.5-900-6%}, the aggregation behavior of a relatively small number of catalysts that were dispersed at high temperature during the activation process led to a decrease in catalytic cracking activity and a gradual decrease in the transformation speed of its microscopic carbon structure to the disordered direction, which affected the rapid generation of micropores and mesopores in the particles.

The surface morphology and structural properties of the BC, BPC_{2.5-900}, FBPC_{2.5-900-1%}, FBPC_{2.5-900-2%} and FBPC_{2.5-900-4%} samples were observed by SEM. As shown in Figure 2a, the vascular bundles of bamboo shavings were well preserved after the carbonization process, with macroporous channels ranging in size from 3 μm to 9 μm . After impregnation and activation with the addition of K_2CO_3 , it could be observed that the sample was in the original macropores and the micropores became more abundant. However, after the chemical activation process, which included loading with Fe^{3+} ions in addition to K_2CO_3 impregnation, it could be seen from Figure 2c, d and e that the surface of the sample was rougher and more porous than that of the BC and BPC_{2.5-900} samples, which represented strong evidence of the pore development process. Importantly, there was a change in the inner epidermis surface morphology from a flat and solid surface to a hollow porous structure, as shown in Figure 2a–c, which fully demonstrated the successful preparation of hierarchical porous carbons.

This section provides evidence that the pore characteristics of FBPC can be controlled by the method of loading Fe^{3+} ions and K_2CO_3 activators together. It is worth noting that the well-controllable mesoporous structure and high specific surface area of FBPC can ensure the effective removal of copper ions during the adsorption process. In addition, the successful preparation of FBPC samples with a high mesoporous ratio and the high specific surface area also provides a logical basis for the implementation of the following work.

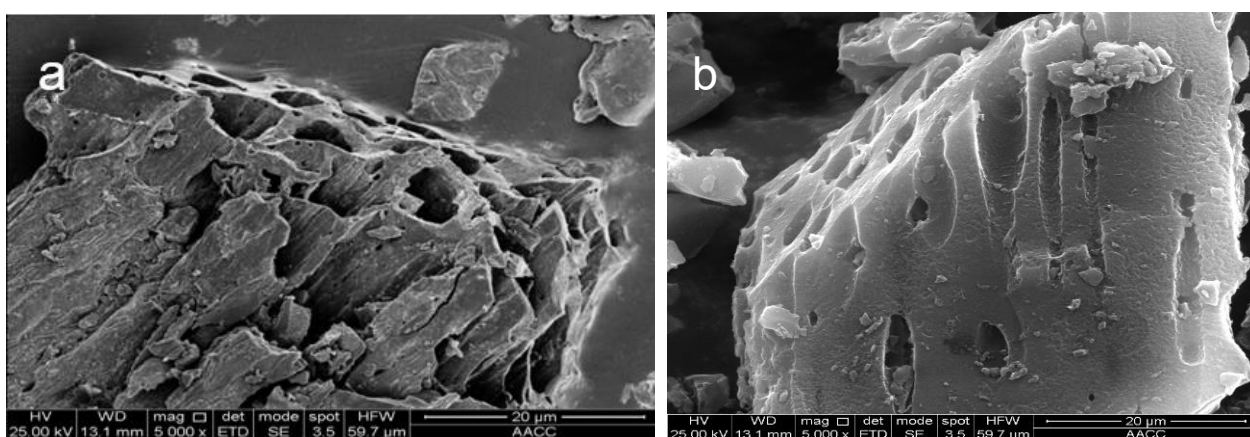


Figure 2. Cont.

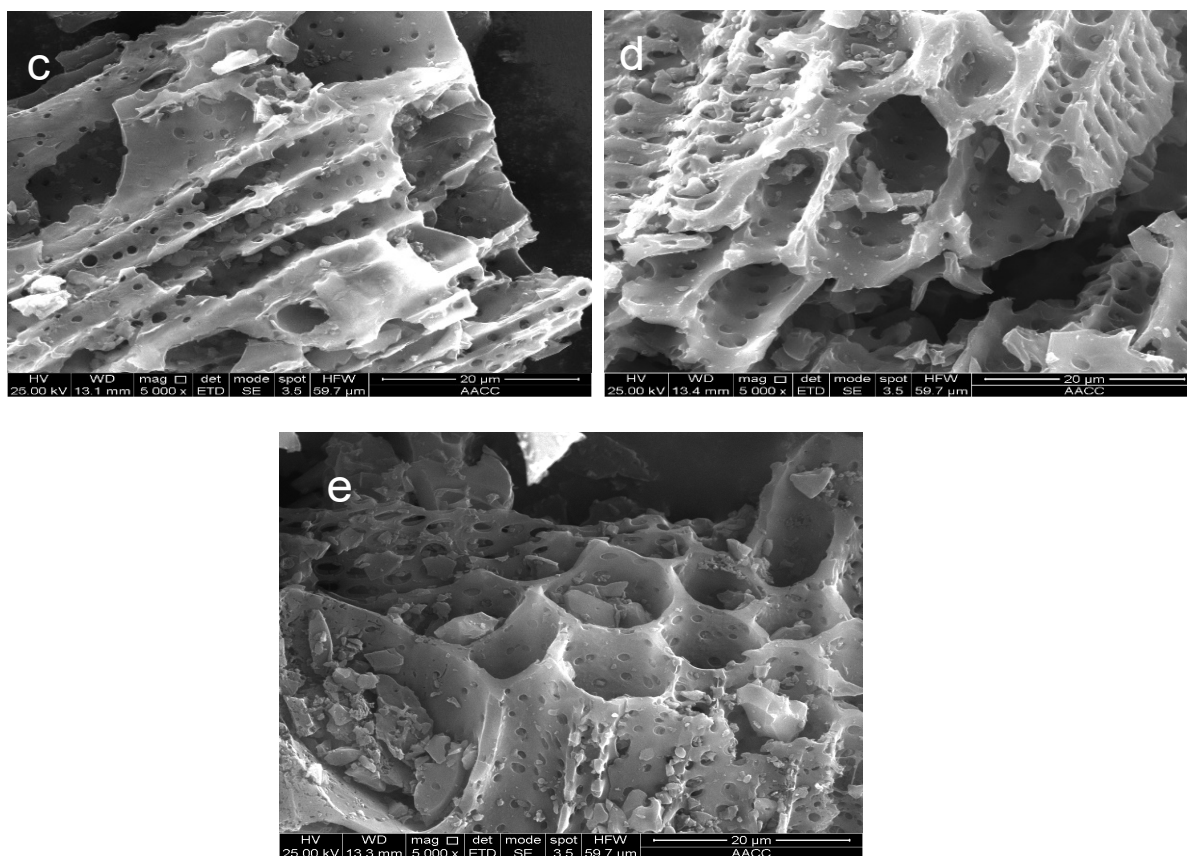


Figure 2. SEM images of (a) BC, (b) BPC 2.5-900, (c) FBPC 2.5-900-1%, (d) FBPC 2.5-900-2% and (e) FBPC 2.5-900-4% with $\times 5000$ magnification.

2.2. Chemical Characteristics

The chemical properties of the adsorbent were studied to understand and explain some of the adsorption phenomena reported in the next section. FTIR analysis is an important means to identify the surface functional groups of adsorbents, which drive the adsorption of heavy metal ions through the chemical mechanism. The characteristic bands of the functional groups of the BC, BPC, and FBPC samples are presented in Figure 3. The wide band of the samples at around 3450 cm^{-1} is ascribed to the O-H stretching mode of hydroxyl groups or adsorbed water. The band observed near 2950 cm^{-1} is attributed to the C-H stretching vibration of $-\text{CH}_2$. With the increase in the preparation temperature, the relative strength of the band decreased, indicating the loss of $-\text{CH}_2$ functional groups in carbon prepared at higher temperatures [26]. A small band in the range of 1500 to 1700 cm^{-1} was found in the sample, which is attributed to the C=O stretching vibration of the ketone, aldehyde, lactone, and carboxyl groups [27,28]. Due to the stretching vibration of the C-O and C-C bond, a band was detected at about 1100 cm^{-1} in all samples [29]. In addition, the peaks in the range of 900 – 650 cm^{-1} represent aromatic C-H bending vibrations [4,30]. The analysis of biochar materials loaded with Fe^{3+} ions showed that the peak at 660 cm^{-1} in biochar materials without Fe^{3+} ions was repressed, suggesting that the surface modification concealed this functionality [31].

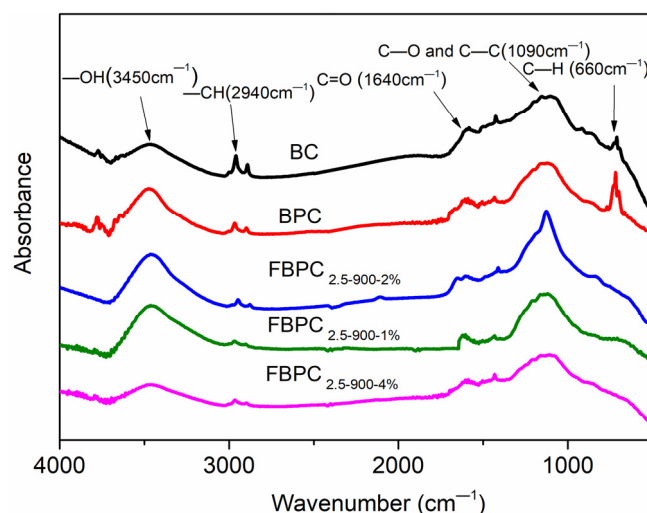


Figure 3. FTIR spectra of the BC, BPC _{2.5-900}, FBPC _{2.5-900-1%}, FBPC _{2.5-900-2%} and FBPC _{2.5-900-2%} samples.

In order to further analyze the thermal stability and composition of BC and FBPC _{2.5-900-2%}, Figure 4 shows the thermogravimetric analysis (TGA) results for the BC and FBPC _{2.5-900-2%} samples in the temperature range from 50 °C to 900 °C, at a fixed heating rate of 10 °C min⁻¹, under nitrogen flow. The pyrolysis process of the BC sample was divided into two stages. The early weightlessness of about 4.6% of the BC, observed at around 310 °C, was due to the loss of water and volatile organic compounds in the microporous structure of the BC [32]. Subsequently, the weight loss curve of the BC sample showed a rapid weight loss of about 35.67% between 310 and 600 °C, which was mainly caused by carbon dioxide being released due to the gradual decomposition of biopolymer components (such as hemicellulose, cellulose, and lignin) [33].

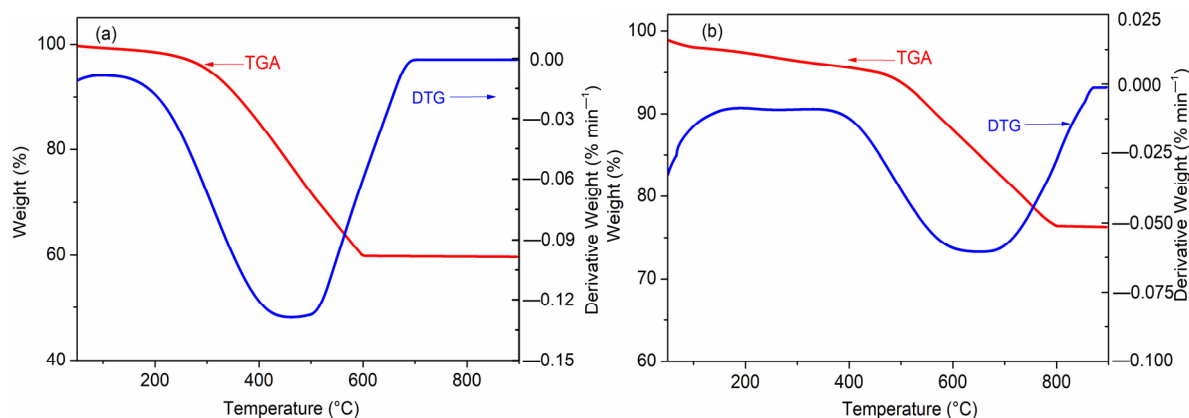


Figure 4. TGA-DTG thermograms for the (a) BC and (b) FBPC _{2.5-900-2%} samples under an N₂ flow that was similar to that of the activation process.

Similarly, the early weight loss of about 6.2% of the FBPC _{2.5-900-2%} was observed at 460 °C due to the presence of water molecules and volatile substances. The early weight loss of FBPC _{2.5-900-2%} was higher than that of the BPC samples, which was caused by the higher water storage of the highly porous structure of the FBPC _{2.5-900-2%} samples. In addition, compared with the BC sample, the weight loss of the FBPC _{2.5-900-2%} sample in the temperature range of 460 to 810 °C was only 26% during the rapid weight loss phase, because the supported iron-based compounds could catalyze the decomposition of all hydrocarbons in biomass carbon and promote the formation and release of volatiles. Therefore, the weight loss of FBPC _{2.5-900-2%} was small, which provides further evidence that the thermal stability of FBPC _{2.5-900-2%} is better than BC.

The research results in this section show that FBPC samples have strong chemical properties and rich functional groups (OH, C-H, C=O, COOH, C-C, and C-O), as well as good thermal stability. These properties can greatly improve the adsorption performance of Cu(II) ions in water.

2.3. Adsorption Studies

According to the characteristics of porosity, three samples of FBPC _{2.5-900-1%}, FBPC _{2.5-900-2%}, and FBPC _{2.5-900-4%} were selected to evaluate the influence of pore properties on Cu(II) adsorption. It can be seen from Table 1 that compared with the other two FBPC samples, FBPC _{2.5-900-2%} had the highest specific surface area ($1996 \text{ m}^2 \text{ g}^{-1}$) and the highest mesoporous ratio ($V_{\text{meso}}/V_{\text{total}} = 0.581$). The experiment on Cu(II) adsorption was carried out in the initial pH range of 2 to 5. Copper could precipitate when the pH was higher than 5, which would interfere with the measurement of Cu(II) in the adsorption process [26,34]. As can be seen from Figure 5, differences in the initial pH values had a significant influence on the adsorption of Cu(II) ions to FBPC _{2.5-900-1%}, FBPC _{2.5-900-2%}, and FBPC _{2.5-900-4%}. Notably, at the lower initial pH values of 2 and 2.5, the adsorption of copper was significantly lower than at the higher pH values. For example, the adsorption capacity of Cu(II) on FBPC _{2.5-900-2%} increased from 165 mg g^{-1} at pH 2 to 220 mg g^{-1} at pH 5. This occurred because the affinity between Cu(II) ions and the adsorbed surface was reduced. In addition, at lower pH values, the competition between H_3O^+ and Cu(II) at exchange sites occurred on the adsorption surface [35]. Additionally, the high solubility and ionization of copper salts in acidic media also led to reduced copper removal efficiency. In addition, as the pH value increased from 3 to 5, the amount of Cu(II) adsorbed on the FBPC adsorbent also increased. This improvement could be attributed to the partial hydrolysis of Cu(II) ions, resulting in the formation of $\text{Cu}(\text{OH})^+$. As previously reported [36,37], $\text{Cu}(\text{OH})^+$ was more adsorptive than Cu^{2+} . More importantly, a possible reason was that when the pH value was higher than 3–4, the hydroxyl (OH) and carboxyl (COOH) groups on the FBPC surface were deprotonated and negatively charged, thereby increasing the attraction of the sample surface to positively charged Cu(II) ions [34,38].

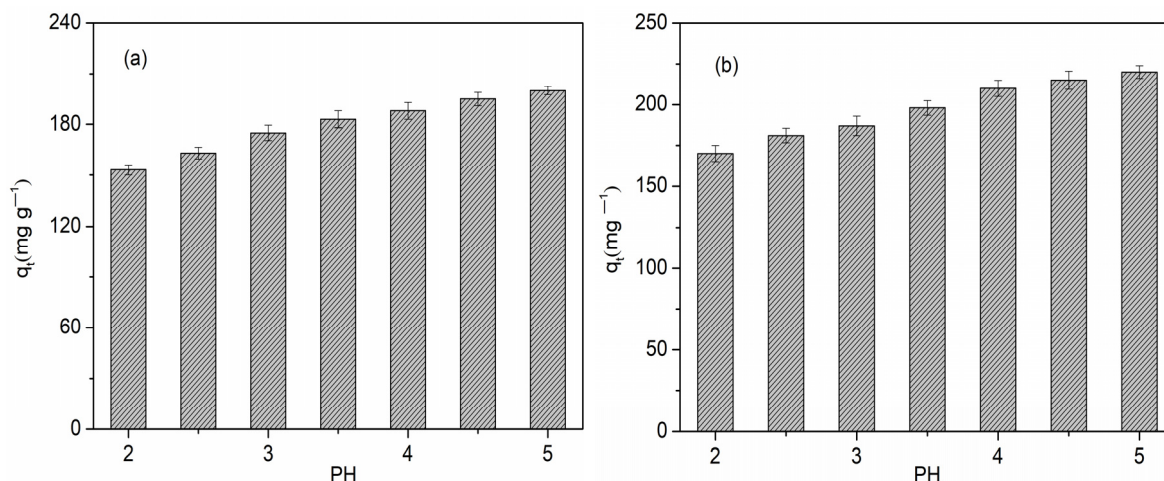


Figure 5. Cont.

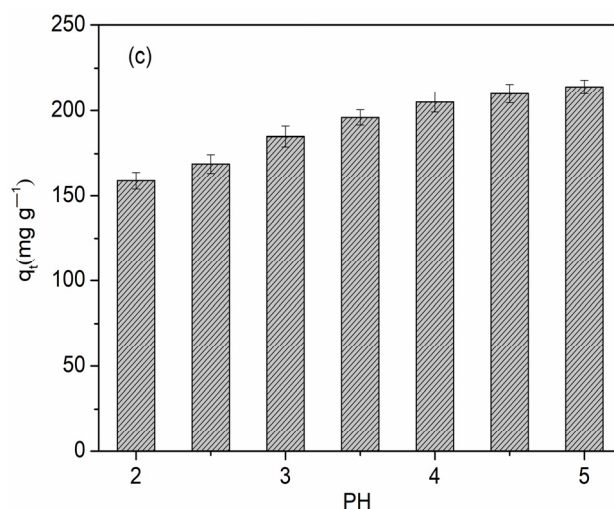


Figure 5. Effect of the initial pH value on Cu(II) adsorption on (a) FBPC 2.5-900-1%, (b) FBPC 2.5-900-2%, (c) FBPC 2.5-900-4%. Adsorbent dose = 0.35 g L⁻¹; shaking time = 120 min; temperature = 298 K; pH = 2–5; shaking speed = 300 rpm; initial Cu(II) concentration = 100 mg L⁻¹.

The adsorption kinetics of Cu(II) ions on three samples, FBPC 2.5-900-1%, FBPC 2.5-900-2%, and FBPC 2.5-900-4%, are shown in Figure 6a–c and Table 2. As shown, Cu(II) adsorption exhibited an initial extremely fast adsorption time, with 80% of the total adsorption occurring within 25 min of the contact time. Then, the amount of copper adsorbed on the three FBPC samples increased slightly before equilibrium was reached. The fast adsorption of the three high-performance carbon adsorbents could be explained by their hierarchical porous structure. It is worth noting that the Cu(II) adsorption process of the FBPC 2.5-900-2% sample reached equilibrium after 70 min, which was much shorter than the adsorption process (100 min) of the FBPC 2.5-900-1% and FBPC 2.5-900-4% samples.

Table 2. Isotherm adsorption parameters for the process of Cu(II) removal by the FBPC samples.

Sample	$q_{e, exp}$ (mg g ⁻¹)	Pseudo-First-Order Equation			Pseudo-Second-Order Equation		
		$q_{e, cal}$ (mg g ⁻¹)	K_1 (L h ⁻¹)	R ²	$q_{e, cal}$ (mg g ⁻¹)	K_2 (g mg ⁻¹ h ⁻¹)	R ²
FBPC 2.5-900-1%	19.90	19.07	0.060	0.9612	20.32	0.007	0.9987
FBPC 2.5-900-2%	27.50	26.70	0.081	0.9425	27.86	0.011	0.9994
FBPC 2.5-900-4%	25.36	25.01	0.074	0.9718	26.10	0.009	0.9995

Note: $q_{e, cal}$: calculated uptake capacity; $q_{e, exp}$: experimental uptake capacity; K : rate constant; R²: correlation coefficient.

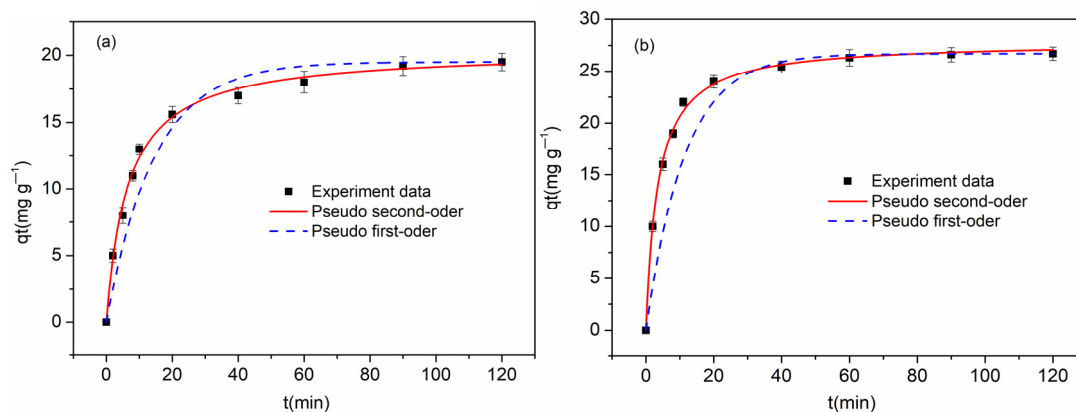


Figure 6. Cont.

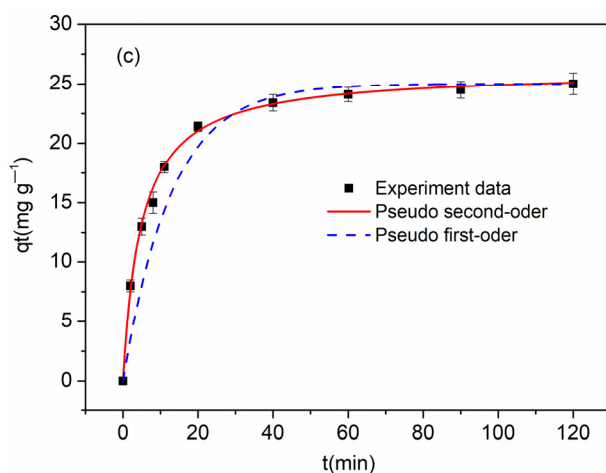


Figure 6. Kinetics of Cu(II) adsorption on (a) FBPC _{2.5-900-1%}, (b) FBPC _{2.5-900-2%}, and (c) FBPC _{2.5-900-4%}. Adsorbent dose = 0.35 g L⁻¹; shaking speed = 300 rpm; shaking time = 5–120 min; initial Cu(II) concentration = 10 mg L⁻¹; pH = 5; and temperature = 298 K.

The adsorption behavior of Cu(II) on the FBPC samples was simulated by using pseudo-first-order and pseudo-second-order nonlinear equations to fit the kinetic data. The mathematical equations of these two models are given in Equations (1) and (2), respectively [39].

$$q_t = q_e \left(1 - e^{-K_1 t}\right) \quad (1)$$

$$q_t = \frac{q_e^2 K_2 t}{1 + q_e K_2 t} \quad (2)$$

where q_e and q_t are the amounts of copper ions adsorbed (mg g⁻¹) on the adsorbent at the equilibrium and at time t , respectively, K_1 (L h⁻¹) is the rate constant of the pseudo-first-order adsorption, and K_2 (g mg⁻¹ h⁻¹) represents the pseudo-second-order adsorption. The kinetic parameters obtained using the pseudo-first-order and pseudo-second-order nonlinear equation fitting are listed in Table 2. It is clear from the above table that the pseudo-first-order equation had a poor fitting degree with the experimental data. On the contrary, the pseudo-second-order model had a better fitting effect, and the fitting coefficient could reach more than 99%. This reflects the fact that the adsorption of Cu(II) on the three FBPC samples was mainly a chemical mechanism [30,34,40]. The k_2 value of FBPC _{2.5-900-2%} was 0.011 g mg⁻¹ h⁻¹, which was significantly higher than those of the FBPC _{2.5-900-1%} and FBPC _{2.5-900-4%} samples (0.007 and 0.009 g mg⁻¹ h⁻¹, respectively). Thus, it could be concluded that the FBPC _{2.5-900-2%} samples, with their high $V_{\text{meso}}/V_{\text{total}}$ ratios, reached adsorption equilibrium more quickly than the FBPC _{2.5-900-1%} and FBPC _{2.5-900-4%} samples. This indicates that a sample having a high mesoporosity ratio causes Cu(II) to be adsorbed more quickly on the sample. The existence of mesopores can provide barrier-free channels for ions to enter the micropores and achieve adsorption on the active sites so that the ions can be quickly transported from the macropores to the active sites in the micropores. In addition, this article also provides an important theoretical basis for studying the adsorption of copper ions on FBPC _{2.5-900-1%}, FBPC _{2.5-900-2%}, and FBPC _{2.5-900-4%} samples. The experimental results were further fitted with the Langmuir and Freundlich isotherms based on the nonlinear Equations (3) and (4) [11].

$$q_e = \frac{q_m K_L C_e}{1 + K_L C_e} \quad (3)$$

$$q_e = K_F C_e^{\frac{1}{n}} \quad (4)$$

where q_m (mg g^{-1}) is the maximum adsorption capacity, K_L (L mg^{-1}) and K_F (mg g^{-1}) are constants for the Langmuir and Freundlich models, respectively, n is the Freundlich constant related to adsorption intensity, and q_e (mg g^{-1}) is the equilibrium adsorption capacity. The adsorption isotherms and parameters of the three FBPC samples are shown in Figure 7a–c and Table 3. As can be seen from the figure, the Langmuir model fits the results better than the Freundlich model and produces a higher correlation coefficient ($R^2 > 96\%$). The results show that the monolayer adsorption of Cu(II) occurred on the homogeneous surface of FBPC samples. From the parameters in Table 3, we can see that the three FBPC samples all showed good Cu(II) ion adsorption capacity, among which the FBPC_{2.5-900-2%} sample had the largest adsorption capacity, up to 256 mg g^{-1} , which was much higher than those of the other two FBPC samples. Therefore, it can be concluded that the higher specific surface area and mesoporous ratios play an important role in the adsorption of Cu(II) ions. The reasons can be listed as follows: firstly, a higher specific surface area can provide more adsorption sites, and secondly, a higher ratio of mesopores can provide barrier-free channels for ions to enter the micropores and achieve adsorption on the active sites, as well as accelerating the transfer of ions from macropores to the velocity of deep active sites in the micropores.

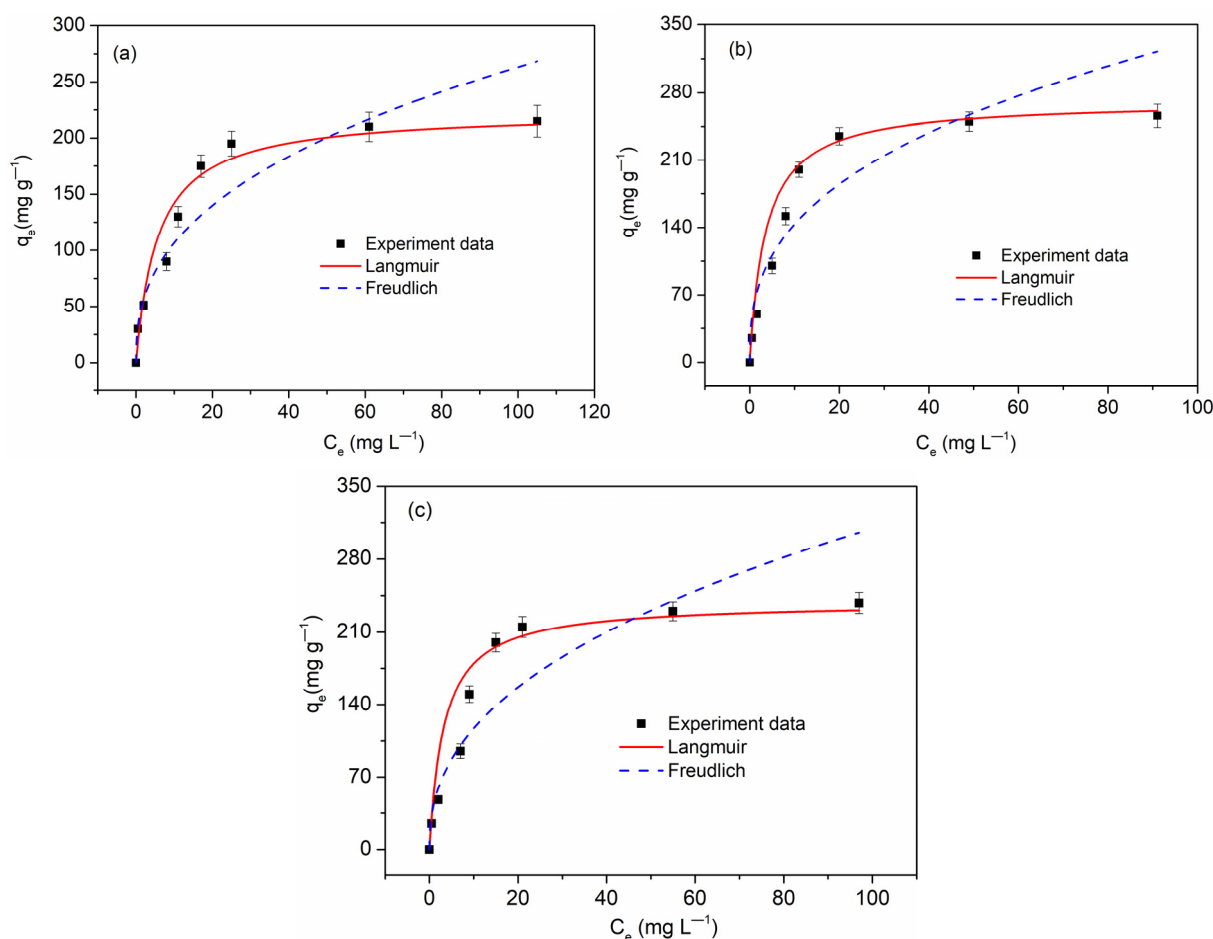


Figure 7. Isotherm of Cu(II) adsorption on (a) FBPC_{2.5-900-1%}, (b) FBPC_{2.5-900-2%}, and (c) FBPC_{2.5-900-4%}. Adsorbent dose = 0.35 g L^{-1} ; shaking time = 90 min; temperature = 298 K; pH = 5.0; shaking speed = 300 rpm; and initial Cu(II) concentration = $10\text{--}200 \text{ mg L}^{-1}$.

Table 3. Kinetic adsorption parameters for the process of Cu(II) removal by the FBPC samples.

Sample	Langmuir			Freundlich		
	q_m (mg g^{-1})	K_L (L g^{-1})	R^2	K_F (mg g^{-1})	n (L g^{-1})	R^2
FBPC 2.5-900-1%	221	0.21	0.96	43.15	2.54	0.87
FBPC 2.5-900-2%	256	0.30	0.97	61.53	2.72	0.91
FBPC 2.5-900-4%	238	0.27	0.96	44.25	2.36	0.89

In previous studies [41], bamboo-based activated carbon was prepared by unloading Fe ions and directly using K_2CO_3 chemical activation steps, and a material with a specific surface area of $1264 \text{ m}^2 \text{ g}^{-1}$ was obtained. The material prepared by loading Fe^{3+} ions prior to activation in this study has a larger specific surface area than the material obtained by Zhang et al. [41]. This shows that the loading of metal Fe^{3+} ions has an important effect on improving the specific surface area and mesopore ratio of bamboo-based activated carbon. The observed Cu(II) adsorption capacity is compared with those of other activated carbon adsorbents prepared from biomass sources described in the literature in Table 4. As can be seen, the FBPC samples prepared in this paper have much higher adsorption capacities and faster adsorption kinetics than other adsorbents. Due to its unique properties (such as high specific surface area, hierarchical porous structure, and high ratio of mesopore to total pore volume), FBPC samples can achieve high-performance adsorption of Cu(II) ions. Therefore, biomass-activated carbon prepared through the loading of Fe^{3+} ions to regulate the pore structure can become a promising copper ion adsorbent in the process of chemical activation.

Table 4. Comparison of maximum adsorption properties of different adsorbents for Cu(II).

Adsorbent	S_{BET} ($\text{m}^2 \text{ g}^{-1}$)	V_{total} ($\text{cm}^3 \text{ g}^{-1}$)	Functional Group	Maximum Capacity (mg g^{-1})	Equilibrium Time (min)	Reference
Chestnut shell-activated carbon	1319	0.57	-OH, C-H, C=C, C=O	98	120	[42]
Grape bagasse-activated carbon	1455	0.88	-OH, C-H, C=C, C=O	44	180	[34]
Rice husk-activated carbons	232	0.15	-OH, C-H, -CH ₂ , C=O, C=C	21	1440	[26]
Hazelnut shell-activated carbon	1651	1.38	—	239	120	[43]
Bamboo shaving-activated carbon	1996	1.571	-OH, C-H, C-C, C=O, C-O	256	70	This work

3. Materials and Methods

3.1. Preparation of Bamboo Powder Biochar and BPC

Bamboo powder was collected from the Sichuan bamboo chopsticks processing plant (Sichuan Province in China) and washed with distilled water several times to remove dust and some impurities. The cleaned bamboo powder was dried at $105 \text{ }^\circ\text{C}$ for 24 h, and then fully dried for subsequent use. Then, the bamboo powder was pyrolyzed under nitrogen atmosphere at $600 \text{ }^\circ\text{C}$ for 2 h to prepare bamboo powder biochar (denoted as BC). BC was impregnated with Potassium Carbonate at different K_2CO_3 : BC mass ratios of 1, 2, 2.5, 3, or 3.5 and dried at $105 \text{ }^\circ\text{C}$ in an electrical oven (denoted BPC). Next, it was activated at $700 \text{ }^\circ\text{C}$, $800 \text{ }^\circ\text{C}$, $900 \text{ }^\circ\text{C}$ and $1000 \text{ }^\circ\text{C}$ (heating rate of $5 \text{ }^\circ\text{C min}^{-1}$) for 2 h in an N_2 atmosphere. Then, it was neutralized with a 1 M hydrochloric acid aqueous solution and filtered and washed several times with distilled water until the filtrate pH was 7. Finally, BPC was collected

after drying at 105 °C for 24 h. The BPC samples, prepared under different conditions, are recorded as BPC X - Y , where X is the ratio of K_2CO_3 to BPC and Y (°C) is the temperature.

3.2. Preparation of Hierarchical Porous Carbon Catalyzed by Fe^{3+} Ions

BC was impregnated at K_2CO_3 :BC mass ratio 2.5, and then 1%, 2%, 4%, 6%, $FeCl_3$ was added (the mass ratio of $FeCl_3$:BC was 1%, 2%, 4%, 6%); it was then impregnated through stirring at room temperature for 12 h, and dried in an electric oven at 105 °C. In the N_2 atmosphere, it was activated at 900 °C for 2 h. Then, the powder was neutralized with a 1 M hydrochloric acid aqueous solution, and then filtered and washed several times with distilled water until the filtrate pH was 7. Finally, FBPC was collected after drying at 105 °C for 24 h. The FBPC samples, prepared under different conditions, are recorded as FBPC 2.5-900- Z , where Z is the amount of $FeCl_3$ added.

3.3. Material Characterization

The specific surface area and pore size distribution of the FBPC samples were characterized using N_2 adsorption–desorption isotherms at 77 K using a Physical adsorption instrument (Quantachrome, autosorb-iQ-2MP, Boynton Beach, FL, USA); the specific surface area (S_{BET}) was calculated using the Brunauer–Emmett–Teller (BET) equation. The density functional theory (DFT) was used to analyze the pore size distribution of the carbon materials. The morphology of the adsorbent was characterized using emission scanning electron microscopy (FE-SEM, S-4800). Using a thermogravimetric (TG) analyzer (PerkinElmer, STA 8000, Waltham, MA, USA) under an N_2 atmosphere, the thermal stability of the preparation of FBPC samples was evaluated. Fourier Transform Infrared Spectroscopy (FT-IR), in the range of 4000–400 cm^{-1} (Nicolet iS10, Thermo Scientific (Waltham, MA, USA)), was used to study the functional groups on the FBPC surface.

3.4. Adsorption Experiments

The adsorption of copper ions onto FBPC samples was investigated. All batch experiments were carried out in a 50 mL centrifuge tube with 30 mL solution at a speed of 300 rpm at 298 K. The Cu(II) solutions were prepared by dissolving $CuSO_4 \cdot 5H_2O$ in distilled water. Kinetic studies were conducted with a 10 $mg L^{-1}$ Cu(II) solution (pH = 5) and 10 mg FBPC, and samples were collected at time intervals from 5 min to 120 min. For adsorption isotherms, different initial Cu(II) ion concentrations (10–200 $mg L^{-1}$) were agitated with 0.35 $g L^{-1}$ dosages of adsorbent in a shaker at 300 rpm for 90 min. Because the copper began to precipitate at pH values of above 6, the effect of the initial solution of pH was conducted with the pH range of 2 to 5. The pH values were adjusted by 0.1 M HCl and 0.1 M NaOH. After reaching equilibrium, the suspension was filtered with a 0.45 μm membrane to obtain the required supernatant. The equilibrium concentration of heavy metal ions in the supernatant was measured using atomic absorption spectroscopy. The adsorptive capacity of Cu(II) was calculated using Equation (5) as follows:

$$q_e = \frac{(C_0 - C_e)V}{W} \quad (5)$$

where C_0 ($mg L^{-1}$) and C_e ($mg L^{-1}$) are the initial and equilibrium adsorbate concentrations in the solution, q_e ($mg L^{-1}$) is the adsorption amount of Cu(II) at equilibrium, W is the mass of the FBPC sample (g), and V is the volume of the solution (L).

4. Conclusions

In this study, a series of FBPC samples with high specific surface area and high mesoporous ratio were successfully synthesized using BC as raw material through Fe^{3+} ion-supported catalysis and a chemical activation process. These steps are essential to achieve efficient adsorption of Cu(II) ions. By adjusting different K_2CO_3 impregnation ratios, as well as the activation temperature and the Fe^{3+} ion loading, the specific surface area, total pore volume and mesoporosity of the catalyst can be well controlled. The results show

that the specific surface area of FBPC_{2.5-900-2%} is 1996 m²g⁻¹, and the mesoporous ratio is 58.1%. The most obvious finding of this study is that FBPC samples synthesized from activated biochar can obtain high adsorption capacity and rapid removal of copper ions. The large specific surface area can ensure a high adsorption capacity, and the mesopores are more conducive to faster ion removal during the adsorption process. Among them, the maximum adsorption capacity of FBPC_{2.5-900-2%} is 256 mg g⁻¹, and its good pore characteristics (hierarchical porous structure, with high $V_{\text{meso}}/V_{\text{total}}$ ratio) are better than the values given in the literature. The research results show that the high specific surface area and high mesoporous structure of bamboo powder biochar are beneficial in terms of achieving high copper adsorption performance.

Author Contributions: Conceptualization, Y.Z., G.Q. and J.W.; data curation, R.W.; funding acquisition, J.W.; investigation, Y.Z., G.Q., R.W. and F.G.; methodology, Y.Z.; project administration, J.W.; software, Y.G.; visualization, Y.G.; writing—original draft, Y.Z. and G.Q.; writing—review and editing, J.W. All authors have read and agreed to the published version of the manuscript.

Funding: This work was supported by the Fundamental Research Funds for the Central Universities (No. 2017QNA25).

Institutional Review Board Statement: Not applicable.

Informed Consent Statement: Not applicable.

Data Availability Statement: Not applicable.

Acknowledgments: This work was supported by the Fundamental Research Funds for the Central Universities (No. 2017QNA25).

Conflicts of Interest: The authors declare no conflict of interest.

Sample Availability: Samples of the compounds are available from the authors.

References

1. Rocha, G.S.; Tonietto, A.E.; Lombardi, A.T.; Melao, M.D.G.G. Effect of copper contaminated food on the life cycle and secondary production of *Daphnia laevis*. *Ecotoxicol. Environ. Saf.* **2016**, *133*, 235–242. [[CrossRef](#)] [[PubMed](#)]
2. Ajmal, M.; Khan, A.H.; Ahmad, S.; Ahmad, A. Role of sawdust in the removal of copper(II) from industrial wastes. *Water Res.* **1998**, *30*, 3085–3091. [[CrossRef](#)]
3. Bilal, M.; Shah, J.A.; Ashfaq, T.; Gardazi, S.; Tahir, A.A.; Pervez, A.; Haroon, H.; Mahmood, Q. Waste biomass adsorbents for copper removal from industrial wastewater—A review. *J. Hazard. Mater.* **2013**, *263*, 322–333. [[CrossRef](#)] [[PubMed](#)]
4. Ss, A.; Cb, B.; Ed, B.; Jp, A. High efficiency removal of heavy metals using tire-derived activated carbon vs commercial activated carbon: Insights into the adsorption mechanisms. *Chemosphere* **2020**, *264 Pt 1*, 128455.
5. Cséfalvay, E.; Pauer, V.; Mizsey, P. Recovery of copper from process waters by nanofiltration and reverse osmosis. *Desalination* **2009**, *240*, 132–142. [[CrossRef](#)]
6. Christensen, E.R.; Delwiche, J.T. Removal of heavy metals from electroplating rinsewaters by precipitation, flocculation and ultrafiltration. *Water Res.* **1982**, *16*, 729–737. [[CrossRef](#)]
7. Sutcu, H.; Dural, A. The adsorption of lead, copper and nickel ions from aqueous solutions on activated carbon produced from bituminous coal. *Fresenius Environ. Bull.* **2007**, *16*, 235–241.
8. Bouhamed, F.; Elouear, Z.; Bouzid, J. Adsorptive removal of copper(II) from aqueous solutions on activated carbon prepared from Tunisian date stones: Equilibrium, kinetics and thermodynamics. *J. Taiwan Inst. Chem. Eng.* **2012**, *43*, 741–749. [[CrossRef](#)]
9. Aydın, H.; Bulut, Y.; Yerlikaya, Ç. Removal of copper (II) from aqueous solution by adsorption onto low-cost adsorbents. *J. Environ. Manag.* **2008**, *87*, 37–45. [[CrossRef](#)]
10. Feng, C.; Chen, Y.A.; Yu, C.P.; Hou, C.H. Highly porous activated carbon with multi-channeled structure derived from loofa sponge as a capacitive electrode material for the deionization of brackish water. *Chemosphere* **2018**, *208*, 285–293. [[CrossRef](#)]
11. Fu, Y.; Shen, Y.; Zhang, Z.; Ge, X.; Chen, M. Activated bio-chars derived from rice husk via one- and two-step KOH-catalyzed pyrolysis for phenol adsorption. *Sci. Total Environ.* **2018**, *646*, 1567–1577. [[CrossRef](#)] [[PubMed](#)]
12. Ge, X.; Ma, Y.; Song, X.; Wang, G.; Zhang, H.; Zhang, Y.; Zhao, H. β -FeOOH nanorods/carbon foam based hierarchically porous monolith for highly effective arsenic removal. *ACS Appl. Mater. Interfaces* **2017**, *9*, 13480. [[CrossRef](#)]
13. Dutta, S.; Bhaumik, A.; Wu, C.W. Hierarchically porous carbon derived from polymers and biomass: Effect of interconnected pores on energy applications. *Energy Environ. Sci.* **2014**, *7*, 3574–3592. [[CrossRef](#)]
14. Sun, J.; Zhang, Z.; Ji, J.; Dou, M.; Wang, F. Removal of Cr⁶⁺ from wastewater via adsorption with high-specific-surface-area nitrogen-doped hierarchical porous carbon derived from silkworm cocoon. *Appl. Surf. Sci.* **2017**, *405*, 372–379. [[CrossRef](#)]

15. Yin, W.; Dai, D.; Hou, J.; Wang, S.; Wu, X.; Wang, X. Hierarchical porous biochar-based functional materials derived from biowaste for Pb(II) removal. *Appl. Surf. Sci.* **2019**, *465*, 297–302. [[CrossRef](#)]
16. Soltani, N.; Bahrami, A.; Pech-Canul, M.I.; Gonzalez, L.A. Review on the physicochemical treatments of rice husk for production of advanced materials. *Chem. Eng. J.* **2014**, *264*, 899–935. [[CrossRef](#)]
17. Xia, Y.; Li, Y.; Gu, Y.; Jin, T.; Yang, Q.; Hu, J.; Liu, H.; Wang, H. Adsorption desulfurization by hierarchical porous organic polymer of poly-methylbenzene with metal impregnation. *Fuel* **2016**, *170*, 100–106. [[CrossRef](#)]
18. He, X.; Zhao, N.; Qiu, J.; Xiao, N.; Yu, M.; Yu, C.; Zhang, X.; Zheng, M. Synthesis of hierarchical porous carbons for supercapacitors from coal tar pitch with nano-Fe₂O₃ as template and activation agent coupled with KOH activation. *J. Mater. Chem. A* **2013**, *1*, 9440–9448. [[CrossRef](#)]
19. Xu, W.-C.; Tomita, A. The effects of temperature and residence time on the secondary reactions of volatiles from coal pyrolysis. *Fuel Process. Technol.* **1989**, *21*, 25–37. [[CrossRef](#)]
20. Öztaş, N.; Yürüm, Y. Pyrolysis of Turkish Zonguldak bituminous coal. Part 1. Effect of mineral matter. *Fuel* **2000**, *79*, 1221–1227. [[CrossRef](#)]
21. Rodriguez Correa, C.; Stollovsky, M.; Hehr, T.; Rauscher, Y.; Rolli, B.; Kruse, A. Influence of the Carbonization Process on Activated Carbon Properties from Lignin and Lignin-Rich Biomasses. *ACS Sustain. Chem. Eng.* **2017**, *5*, 8222–8233. [[CrossRef](#)]
22. Yeh, C.L.; Hsi, H.C.; Li, K.C.; Hou, C.H. Improved performance in capacitive deionization of activated carbon electrodes with a tunable mesopore and micropore ratio. *Desalination* **2015**, *367*, 60–68. [[CrossRef](#)]
23. Song, X.; Ying, Z.; Chang, C. Novel Method for Preparing Activated Carbons with High Specific Surface Area from Rice Husk. *Ind. Eng. Chem. Res.* **2012**, *51*, 15075–15081. [[CrossRef](#)]
24. Linares-Solano, C.A. Understanding chemical reactions between carbons and NaOH and KOH: An insight into the chemical activation mechanism. *Carbon* **2003**, *41*, 267–275.
25. Bedia, J.; Belder, C.; Ponce, S.; Rodriguez, J.; Rodriguez, J.J. Adsorption of antipyrine by activated carbons from FeCl₃-activation of Tara gum. *Chem. Eng. J.* **2018**, *333*, 58–65. [[CrossRef](#)]
26. Zhang, J.; Hao, F.; Lu, X.; Jie, T.; Xu, X. Removal of Cu(II) from aqueous solution using the rice husk carbons prepared by the physical activation process. *Biomass Bioenergy* **2011**, *35*, 464–472. [[CrossRef](#)]
27. Kennedy, L.J.; Vijaya, J.J.; Sekaran, G. Effect of Two-Stage Process on the Preparation and Characterization of Porous Carbon Composite from Rice Husk by Phosphoric Acid Activation. *Ind. Eng. Chem. Res.* **2004**, *43*, 1832–1838. [[CrossRef](#)]
28. Tian, Q.; Zhang, Y.; Li, G.; Wang, Y. Flocculation of ultrafine coal slimes achieved by flotation column. *Energy Sources* **2017**, *39*, 899–904. [[CrossRef](#)]
29. Lambert, A.; Drogui, P.; Daghrir, R.; Zaviska, F.; Benzaazoua, M. Removal of copper in leachate from mining residues using electrochemical technology. *J. Environ. Manag.* **2014**, *133*, 78–85. [[CrossRef](#)]
30. Liu, N.; Zhang, Y.; Xu, C.; Liu, P.; Wang, Q. Removal mechanisms of aqueous Cr(VI) using apple wood biochar: A spectroscopic study. *J. Hazard. Mater.* **2019**, *384*, 121371. [[CrossRef](#)]
31. Zhang, P.; O'Connor, D.; Wang, Y.; Jiang, L.; Hou, D. A green biochar/iron oxide composite for methylene blue removal. *J. Hazard. Mater.* **2019**, *384*, 121286. [[CrossRef](#)]
32. Muniandy, L.; Adam, F.; Mohamed, A.R.; Ng, E.-P. The synthesis and characterization of high purity mixed microporous/mesoporous activated carbon from rice husk using chemical activation with NaOH and KOH. *Microporous Mesoporous Mater.* **2014**, *197*, 316–323. [[CrossRef](#)]
33. Demirbas, A. Effect of temperature on pyrolysis products from four nut shells. *J. Anal. Appl. Pyrolysis* **2006**, *76*, 285–289. [[CrossRef](#)]
34. Demiral, H.; Güngör, C. Adsorption of copper(II) from aqueous solutions on activated carbon prepared from grape bagasse. *J. Clean. Prod.* **2016**, *126*, 103–113. [[CrossRef](#)]
35. Ca Rpio, I.M.; Machado-Santelli, G.; Sakata, S.K.; Filho, S.F.; Rodrigues, D.F. Copper removal using a heavy-metal resistant microbial consortium in a fixed-bed reactor. *Water Res.* **2014**, *62*, 156–166. [[CrossRef](#)]
36. Larous, S.; Meniai, A.H.; Lehocine, M.B. Experimental study of the removal of copper from aqueous solutions by adsorption using sawdust. *Desalination* **2005**, *185*, 483–490. [[CrossRef](#)]
37. Chen, J.; Clark, M.; Yan, Y. Adsorption of copper to different biogenic oyster shell structures. *Appl. Surf. Sci.* **2014**, *311*, 264–272.
38. Drage, T.C. Activated Carbon Adsorption, Roop Chand Bansal, Goyal Meenakshi, CRC Press, Taylor & Francis Group (2005), pp. 520, Hardback, \$170.96, ISBN: 0-8247-5344-5. *Fuel* **2007**, *86*, 313.
39. Revellame, E.D.; Fortela, D.L.; Sharp, W.; Hernandez, R.; Zappi, M. Adsorption kinetic modeling using pseudo-first order and pseudo-second order rate laws: A review. *Clean. Eng. Technol.* **2020**, *1*, 100032. [[CrossRef](#)]
40. Lyu, H.; Tang, J.; Huang, Y.; Gai, L.; Zeng, E.Y.; Liber, K.; Gong, Y. Removal of hexavalent chromium from aqueous solutions by a novel biochar supported nanoscale iron sulfide composite. *Chem. Eng. J.* **2017**, *322*, 516–524. [[CrossRef](#)]
41. Zhang, J.; Zhong, Z.; Guo, H.; Jiang, X. Preparation of Bamboo-Based Activated Carbon. In Proceedings of the 2010 Asia-Pacific Power and Energy Engineering Conference, Chengdu, China, 28–31 March 2010.
42. Oezcimen, D.; Ersoy-Mericboyu, A. Removal of copper from aqueous solutions by adsorption onto chestnut shell and grapeseed activated carbons. *J. Hazard. Mater.* **2009**, *168*, 1118–1125. [[CrossRef](#)] [[PubMed](#)]
43. Milenković, D.D.; Dašić, P.V.; Veljković, V.B. Ultrasound-assisted adsorption of copper(II) ions on hazelnut shell activated carbon. *Ultrason. Sonochem.* **2009**, *16*, 557–563. [[CrossRef](#)] [[PubMed](#)]